Introducing multi-energy ratios as an alternative to multi-energy calibration for Br determination *via* high-resolution continuum source graphite furnace molecular absorption spectrometry. A case study

Raúl Garde, Flávio V. Nakadi,* Esperanza García-Ruiz and Martín Resano*

Department of Analytical Chemistry, Aragón Institute of Engineering Research (I3A), University of Zaragoza, Pedro Cerbuna 12, 50009, Zaragoza, Spain. E-mail: mresano@unizar.es; E-mail: flavionakadi@gmail.com

Abstract

This manuscript explores the advantages of using multi-signal calibration approaches for the determination of non-metals *via* high-resolution continuum source graphite furnace molecular absorption spectrometry (HR CS GFMAS), targeting Br as an example. Besides multi-energy calibration (MEC), a novel approach deriving from it, multi-energy ratios (MER), is introduced and compared under different conditions. This approach makes use of the same data but in a different way, such that no linear regression is performed; instead, ratios are calculated.

The article investigates the potential errors deriving from the use of amounts of spike dissimilar from the sample content, leading to too high (close to 1) or too low (close to 0) slopes/ratios, setting the best conditions in terms of precision and accuracy for the intended determination in the range of approx. 0.5 to 0.6. Also, situations where the use of MER could be recommended over MEC are identified: namely when only a few transitions of sufficient sensitivity and free

from overlaps are available or else, many transitions but of similar sensitivity, which may occur when HR CS GFMAS is deployed. Otherwise, for multiple transitions covering a wider sensitivity range, use of linear regression and thus, of MEC, seems favoured, as a better precision can be achieved. The calculation of limits of detection and quantification for both approaches is also discussed.

It is finally further demonstrated that these multi-signal strategies help in solving chemical interferences, which very often hamper the determination of non-metals with HR CS GFMAS, and they do so in a simple way, without the need for laborious work or for the preparation of several standards and sample aliquots, therefore making them a very intriguing option when this technique is deployed.

1. Introduction

Quantitative methods of analysis depend on the relation between the signal of the analyte and the concentration of such analyte in a sample, a relation that should be either known in advance *via* theoretical considerations without the use of any analytical standard of known concentration (absolute methods), or else experimentally established using analytical standard(s). In instrumental analysis, many efforts have been directed at the development of absolute methods.[1,2] However, in the end, the most popular strategies depend on external calibration based on linear regression statistics, a method that fits the data to a linear curve minimizing the error in the Y-axis (analytical signal), since the error in the X-axis (analyte concentration or total amount) is considered as negligible in comparison. But the presence of the matrix in the sample can affect the analytical signal, due to the occurrence of interferences. Use of internal standards is a widely accepted approach to minimize such interferences to some extent, although it cannot always be used as monitoring two different signals at the same time sometimes is not possible. Alternative calibration approaches such as standard addition or matrix-matching show the potential to correct for some of these matrix-related interferences.[3-6] These approaches provide some benefits but also come with some drawbacks, such as requiring more effort, resulting in a lower sample throughput, and, in the case of matrix-matching, the necessity to know or determine the presence of some compounds to replicate such matrix.

Alternatively, in the case of using techniques in which the signal of different isotopes can be selectively measured, isotope dilution is a powerful approach. Unlike the methods discussed before, isotope dilution mass spectrometry does not rely on linear regression. Instead, the well-known natural abundances of the

stable isotopes are considered “true”, or else, their relation can be experimentally measured. A spike of the target species that shows a substantially different isotopic composition from the natural one is also required. Typically, by measuring two isotopes free from spectral overlaps of the target species in an aliquot of the sample, an aliquot of the spike and an aliquot of an isotopically equilibrated mixture of sample plus spike (blend), the signals from such isotopes can be ratioed and from those values the analyte content in the sample can be derived.[7] This methodology is considered a primary analytical technique due to its high precision and potential to correct for matrix effects.[8,9] However, it is not always possible to make use of it, among other reasons simply because in elemental analysis the target analyte may not possess more than one stable isotope.

Recently, a new calibration methodology has been introduced by Virgilio *et al*.[10] This strategy exploits the monitorization of several “channels” (*i.e.*, energetic transitions; isotopes; polyatomic species) of the same analyte of two aliquots: sample spiked with a blank (sample+blank) and sample spiked with a known amount of analyte (sample+standard). By plotting the signals from such aliquots and performing linear regression, the mass or concentration of the sample can be calculated using the slope of such linear regression (see section 3.1.1. for more details).

This represents an ingenious approach with potential to overcome matrix interferences without the need for performing extra measurements. In fact, the number of measurements is actually lower than those needed for a conventional external calibration (unless a one-point calibration is carried out). The advantage

of obtaining multiple signals from every aliquot replaces the need to prepare and measure many standards.

This approach was labelled multi-energy calibration (MEC) and it has been used for atomic emission techniques such as inductively coupled plasma optical emission spectrometry (ICP OES),[10] microwave-induced plasma optical emission spectrometry (MIP OES)[10,11] and laser-induced breakdown spectrometry,[12-16] as well as for atomic absorption processes, namely high-resolution continuum source flame atomic absorption spectrometry (HR CS FAAS),[10] high-resolution continuum source molecular absorption spectrometry (HR CS MAS)[17] and molecular absorption in the ultraviolet-visible region of the spectra, in addition to fluorescence.[18]

The same principle has also been applied to inductively coupled plasma mass spectrometry (ICP-MS) by monitoring different isotopes from the same element,[19,20] and then it has been referred to as multi-isotope calibration. Moreover, since not all elements possess various stable nuclides, the use of a reaction cell to form and measure different adducts from the only nuclide available in such cases has also been proposed, taking advantage of the potential of inductively coupled plasma tandem mass spectrometry in this regard.[21,22] This certainly represents an innovative approach to further expand the use of this calibration approach, and then it has been named as multispecies calibration.[23]

Most of these papers demonstrate the application of this multi-signal calibration concept to develop applications with different techniques, further proving its promising performance. However, owing to its novelty, there is a lack of fundamental knowledge regarding its optimal use. For instance, as will be shown in section 3.1.1, the relationship between the slope of the regression and the

concentration of the analyte is not linear, which implies that the amount of spike added may play an important role in terms of precision and accuracy.

A very recent work by Virgilio *et al.* has investigated some of these fundamental aspects, namely how to properly calculate the limits of detection (LOD) and quantification (LOQ) as well as indicating a working range for the slope in which good accuracy and precision are expected.[24] While this is a welcome addition, we believe there are still fundamental aspects that require further investigation for an optimal application of the methodology to each particular situation.

In our view, one of the techniques that can benefit more from the use of this intriguing calibration strategy is HR CS MAS in general and, in particular, when graphite furnace is used (HR CS GFMAS) as vaporizer.[25,26] The reason for this is that such technique is very prone to suffer from chemical interferences deriving from the presence of other elements in the sample. Generally, the vaporization process is often not as straightforward as a pure atomization process mostly based on temperature, and the presence of many other species may result in the formation of other compounds different from the targeted one.[27,28] Interestingly, while commercially available HR CS AAS instrumentation offers the potential to monitor only a narrow part of the spectrum simultaneously, which affects the multi-element possibilities of the technique,[29,30] when molecular species are measured different rotational or vibrational transitions superimposed to the electronic transitions are monitored,[31,32] and the resolution of the instrumentation is often sufficient to resolve such transitions. In other words, when HR CS MAS is used, often many lines can be fully simultaneously monitored, which can make MEC an ideal strategy to minimize matrix effects as well as to increase sample throughput. In this aspect, MEC has only been applied to HR CS MAS once, when

Vieira *et al.*[17] studied the determination of N, P and S in fertilizers (N and P) and commercial salts (S and N) by HR CS FMAS *via* the measurement of the molecules NO, PO and CS, respectively, and the determination of Cl in milk *via* the measurement of CaCl by HR CS GFMAS, with positive results.

This study has selected the CaBr molecule to develop a method for the determination of Br using HR CS GFMAS, with the goal to discuss fundamental aspects related with the application of MEC as calibration approach (error propagation as a function of the slope selected, selection of lines, linearity and calculation of LODs) when such technique is applied. Moreover, another different approach, similar to MEC in terms of the aliquots that need to be measured, but different in terms of data processing is introduced. This new strategy can be considered as inspired by isotope dilution as it is also based on calculating ratios (see section 3.1.2.), and the name proposed for it is multi-energy ratios (MER).

The selection of both Br as analyte and of CaBr as target molecule where certainly not fortuitous. The formation of this molecule or of any other Br molecule is easily affected by chemical interferences,[27,33] so it is a challenging problem to solve with MEC or MER approaches, as will be discussed. Moreover, CaBr offers transitions of different characteristics in two different spectral regions, such that pros and cons of these two approaches can be properly evaluated.

2. Experimental

2.1. Instrumentation

All the measurements were carried out using a contrAA 800G high-resolution continuum source atomic absorption spectrometer (Analytik Jena AG, Jena, Germany) equipped with transversally-heated graphite tube atomizers that incorporated a platform (Analytik Jena AG). The main details about this type of

instrument can be found elsewhere.[25] The samples and reagents were pipetted automatically with an autosampler ASGF (Analytik Jena AG).

2.2. Standards, reagents and samples

The solutions were prepared with reagents of analytical grade or higher purity. Deionized water purified by a Milli-Q system (Millipore, Bedford, USA) was used for the solutions. Nitric acid 65% Suprapur® (Merck, Darmstadt, Germany) was diluted to 1% v v^{-1} to prepare the chemical modifier and molecule-forming reagent solutions.

A 1000 mg L^{-1} Br standard (Merck) was used to prepare all the Br aqueous standard solutions, as sample and/or spike. A Pd standard solution 10 g L^{-1} (Merck) was diluted in order to achieve a final mass of 30 μg (5 μL of 6 g L^{-1} Pd solution). Calcium carbonate with purity of >99.0% (Sigma-Aldrich, St. Louis, USA) was dissolved in HNO_3 1% v v^{-1} until a final concentration of 3% m v^{-1} Ca was obtained, then 5 μL were pipetted together with the sample and chemical modifier (150 μg Ca). The interference study was carried out by proper dilutions of a Cl standard solution 1000 mg L^{-1} (Merck).

The certified reference material (CRM) of water Anions - Whole Volume QC3060 (Lot#LRAB9707, Sigma-Aldrich) was analyzed to evaluate the accuracy of the method and the impact of interfering species.

2.3. Measurement conditions

Two CaBr vibronic transitions were monitored, $X^2\Sigma \rightarrow A^2\Pi$ (0,0) and $X^2\Sigma \rightarrow B^2\Sigma$ (1,0), around 625.0 and 600.5 nm, respectively. Preliminary tests comparing peak height and peak area, with 1, 3 or 5 detector pixels in both cases, showed that using 5 pixels and measuring peak areas (integrated absorbance) resulted

in better linearities obtained *via* MEC. Thus, such approach was selected for this study.

For all the measurements, unless otherwise noted, the temperature program and general conditions of the graphite furnace were adapted from Flórez & Resano[33] and are shown in **Table 1**. Several peaks (wavelengths) of both transitions were evaluated, so they were named after their detection pixel for practical purposes, as shown in **Table 2**. **Figure 1** shows the spectra (average of 68 spectra obtained during 5 s of detection time) of the CaBr diatomic molecule at both wavelengths, labelling the peaks studied with their respective detection pixel.

3. Results and discussion

3.1. Theoretical background

3.1.1. Multi-energy calibration (MEC)

Multi-energy calibration is a novel calibration approach that has been proposed by Virgilio *et al.*[10] for use in optical spectrometry. The calculations corresponding to such approach can be explained as follows: considering the general correlation found in spectrometric techniques, at a specific wavelength (λ_i), the analytical signal $I(\lambda_i)^{Sam}$ is linearly proportional, by the proportionality constant *m*, to the analyte concentration C^{Sam}, as written in equation 1. Obviously, the addition of a spike C^{Std} results in an increase in the analyte level and the instrumental response should also vary accordingly, $I(\lambda_i)^{Sam+Std}$ (see equation 2).

$$I(\lambda_i)^{Sam} = mC^{Sam} \quad (1)$$

$$I(\lambda_i)^{Sam+Std} = m(C^{Sam} + C^{Std}) \quad (2)$$

Combining both equations 1 and 2, equation 3 is obtained, which relates the analytical signal of a sample and a spiked sample with the concentration of the analyte in the sample and in the spike. This equation is convenient because this relation is true when measuring different transitions, occurring at different wavelengths, which possess different sensitivities. Therefore, if the sample and sample+standard can be measured at different wavelengths, and their data are plotted as $I(\lambda_i)^{Sam}$ *versus* $I(\lambda_i)^{Sam+Std}$, a linear plot should be obtained with a slope S equal to ($C^{Sam}/C^{Sam}+C^{Std}$), as shown in equation 4. Rearranging such equation, equation 5 is obtained, which expresses the concentration of the sample as a function of the slope (measurable) and the concentration of the spike (which should be known in advance).

$$I(\lambda_i)^{Sam} = I(\lambda_i)^{Sam+Std}\left[\frac{C^{Sam}}{C^{Sam}+C^{Std}}\right] \quad (3)$$

$$Slope = S = \frac{C^{Sam}}{C^{Sam}+C^{Std}} \quad (4)$$

$$C^{Sam} = \frac{SC^{Std}}{(1-S)} \quad (5)$$

The previous works about MEC usually mix sample+blank (1:1) to balance the dilution originated when the spike is added (1:1). This strategy is useful because the addition of a spike solution into the sample leads to a dilution of the latter. Therefore, if the same volume of both blank and spike solutions is added to the sample, the dilution would be the same in both cases, making it possible to carry out a straightforward calculation, as shown in equation 5.

However, this is not an issue for HR CS GFMAS because this technique typically uses a known-volume. Therefore, it is possible to use the equation 5 also for masses instead of for concentrations. In this work, the amount of analyte

(bromine) will be given as mass, although the terminology C^{Sam} and C^{Std} will be maintained for simplicity. Thus, in the current work, the blank was measured separately and subtracted from the sample and sample+standard analytical signals.

Since the relation evaluated by MEC is the instrumental intensity of the sample *versus* the intensity of the sample+standard, the slope values should be between ~0 (infinite amount of spike added) and ~1 (infinitesimal amount of spike added). In this context, one could predict the theoretical bias of the concentration finally obtained as a function of the deviation of the slope experimentally calculated.

Such deviation can be expressed as the absolute slope measurement error, e_S, which ultimately contributes to the deviation of C^{Sam}, e_C, as described in equation 6.

$$(C^{Sam} \pm e_C) = \frac{(S \pm e_S)C^{Std}}{[1-(S \pm e_S)]} \qquad (6)$$

The theoretical value of C^{Sam} is obtained when $e_S = 0$, *i.e.*, the relation between C^{Sam} and C^{Std} is exactly (S/1–S). Assuming that the variations of C^{Std} are practically negligible, then the deviation when calculating C^{Sam}, *i.e.* e_C, exists due the deviation in the estimation of S, *i.e.* e_S, as detailed in equation 6.

Therefore, it is possible to estimate how the e_S value will affect the concentration bias with equation 7. Basically, the bias reflects the difference between theoretical and experimentally obtained values for (S/1–S), which directly translates into a difference of C^{Sam}. Thus, the % of bias for C^{Sam} can be written as:

$$bias_{C^{Sam}}^{\pm}(\%) = \frac{\left\{\frac{(S \pm e_S)}{[1-(S \pm e_S)]}\right\} - \left(\frac{S}{1-S}\right)}{\left(\frac{S}{1-S}\right)} \times 100\% \qquad (7)$$

It can be noticed (see equation 6) that the upper limit of e_S value will lead to the upper limit of e_C and concentration bias, e_C^+ and $bias_{C^{Sam}}^{\pm}$, respectively. Thus, equation 7 can be further developed into equation 8 (see Supplementary information for more details).

$$bias_{C^{Sam}}^{\pm}(\%) = \frac{e_S}{S(1-S-e_S)} \times 100\% \qquad (8)$$

The lower limit, $bias_{C^{Sam}}^{-}$, can be calculated analogously, resulting in equation 9 (see Supplementary information). Both equations 8 and 9 can be unified and they become equation 10, which enables the calculation of both the upper and lower concentration biases, just applying "+" (for the upper limit) or "– " (for the lower limit) where " $\pm$ " is indicated. For instance, a 5% deviation of the slope, for a slope value of 0.5 (thus S=0.5 and e_S = 0.025) will ultimately result in a concentration bias of 10.5% and –9.5% (depending on whether the deviation is positive or negative, respectively). It is noteworthy that the relation between e_S and $bias_{C^{Sam}}^{\pm}$ is neither linear nor symmetric.

$$bias_{C^{Sam}}^{-}(\%) = \frac{-e_S}{S(1-S+e_S)} \times 100\% \qquad (9)$$

$$bias_{C^{Sam}}^{\pm}(\%) = \frac{\pm e_S}{S(1-S \pm e_S)} \times 100\% \qquad (10)$$

Figure 2 shows the effect of the S value on the calculation of the analyte concentration. All the data of **Figure 2** was obtained theoretically using equation 10. Three deviations of the true slope are displayed for comparison, representing 1, 5 and 10% of deviation. It is evident that high slope values will lead to greater

concentration bias, *e.g.*, for slope of 0.7, a 10% deviation in the experimental calculation of such parameter leads to a difference of approx. 43% in terms of concentration. **Figure 2** shows the curves up to a slope of 0.8 only, because the concentration bias grows substantially for higher values when a 10% deviation in the calculation of the slope is assumed: for a slope of 0.90, the concentration bias rises up to 1000%. In fact, for high deviations and high slopes the model proposed in equation 8 will eventually fail, as the denominator ($1 – S - e_S$) may become negative, which makes no sense as such error is defined as positive.

In any case, these extremely high deviations for high slopes can be explained simply by analyzing equation 5, because as the slope gets closer to 1, the value (1-S) gets closer to zero and any small difference in the estimation of S leads to a large difference in terms of (S/1–S). For instance, for a true value of S = 0.9, obtaining a calculated value of 0.909 represents a difference of only 1%. However, this variation will lead to a (S/1–S) value of 9.99, instead of the true value of 9. Thus, a difference of only 1% is transformed into a final difference of 11% in terms of (S/1–S). Therefore, when designing the experiments with high S values, higher deviations are expected, which would lead to inaccuracies if only one replicate is performed, and to higher irreproducibility when several replicates are carried out.

Figure 2 suggests that using lower slopes (when the amount of analyte in the spike is several times higher than in the sample) would be recommended because the bias will be lower, which in theory is correct. However, such situation could lead to another source of error. For low slopes, the concentration of the analyte in the sample gets to be so low that it shows a minimal influence on the analytical signal, which is certainly not desirable. This effect will be further

discussed in Section 3.2. Virgilio *et al*.[24] recently shown experimentally that use of "extreme conditions" for the slope ($\leq$0.1 or $\geq$0.9) results in lower trueness.

Clearly, the deviation of the MEC slope can lead to a miscalculation of the analyte concentration, as it also occurs for other more conventional calibration strategies. However, MEC also presents another issue that should be considered carefully. The concept of MEC is to plot a graph of instrumental responses (analytical signals), sample (y-axis) *vs*. sample+standard (x-axis), measured at different wavelengths and use linear regression to calculate the slope, which is later substituted in equation 5 to calculate the sample concentration. Therefore, the variables represented in both graph axes show uncertainties associated with the measurements when using MEC, unlike what occurs in a conventional calibration, where the error in the x-axis (mass or concentration) can be considered as negligible.[3] Thus, choosing a suitable linear regression model seems recommended. In this work, the software Origin 2019b was used to calculate the MEC slope and its standard deviation (which can be readily applied for calculating the standard deviation of the analyte content) with a linear fit with x error mode, which minimizes the sum of square of error on both x and y directions, also known as York Method.[34]

3.1.2. Multi-energy ratios (MER)

For MEC, the relation of the analytical signal at different wavelengths with the concentration is described in equation 3, from which equation 5 is derived. Another way to process the data is also possible for which we propose the name of multi-energy ratios (MER). Instead of a linear regression, a direct ratio between both intensities can be calculated. The concentrations will now be related to the ratios (R) of the analytical signals measured at every wavelength (equation 11).

Equation 12 can be derived from equation 11, showing that both ways to process the data, either using the slope (equation 5) or the (equation 12) ratio, are analogous, simply changing the way in which the same data is processed. Therefore, all the considerations made for MEC in Section 3.1.1 are also valid for MER.

$$\frac{I(\lambda_i)^{Sam}}{I(\lambda_i)^{Sam+Std}} = R = \frac{C^{Sam}}{C^{Sam} + C^{Std}} \quad (11)$$

$$C^{Sam} = \frac{RC^{Std}}{(1-R)} \quad (12)$$

Figure 3 shows an example of the same experimental data treated by both methods, MEC and MER. The measurements of 11 transitions were evaluated, from 624.510 to 625.478 nm (pixels 40, 46, 54, 63, 74, 86, 100, 114, 131, 149 and 168, see **Figure 1A** and **Table 2** for more information). The x-axis of **Figure 3B** shows the detection pixels instead of the wavelengths for practical purposes. In this study, the sample was 10 μL of a 3 mg L^{-1} Br standard solution (30 ng Br) and the sample+standard was 20 μL of the same solution (60 ng Br), representing the addition of 10 μL of spike of 3 mg L^{-1} (Br-spike mass 30 ng). The instrumental conditions used are shown in **Table 1**.

MEC shows good correlation among the data, r^2 = 0.9986, and a slope of 0.5515 is calculated with such approach, which deviates by approx. 10% from the theoretically expected slope (0.5). Applying equation 5, the Br sample mass calculated is 36.9 ± 2.6 ng (average value ± standard deviation), which is 23% biased from the actual mass of 30 ng. On the other hand, the average ratio of all 11 transitions was found to be 0.4863, which applying the MER approach results in a value of 28.9 ± 5.4 ng, a 3.6% difference only from the true mass.

One of the advantages of using the MEC strategy is the possibility to detect and eliminate outliers.[10] Visualizing the residual data plot of **Figure 3A**, it is possible to remove the data from pixels 46, 149 and 168, which would lead to a new linear correlation of $r^2 = 0.9975$ and a slope of 0.5670 ± 0.0157. In this case, the calculated Br mass of the sample will be even higher, 39.3 ± 2.5 ng. On the other hand, a conventional linear regression using direct weighing errors with all the 11 transitions was also performed, and in that way MEC leads to a $r^2 = 0.9984$ and a slope of 0.5146 ± 0.0070, and an ultimate Br value of 31.8 ± 0.9 ng. Although in this case this simpler linear regression model provides a slope-value that, calculating the concentration, is less biased, we still propose and will use for further data analysis (unless otherwise noted) a regression model that considers the contribution in terms of uncertainty of both axes for calculating the best linear correlation, as it is more correct considering that in both axes absorption measurements are plotted.

But outliers can also be detected with ease using MER. Evaluating the data for MER in **Figure 3B**, it is clear that the pixels 40 and 54 are far off the ratio average: they differ by 26.6% and 14.4%, respectively, from 0.4863. If they are considered as outliers, the resulting average ratio is 0.5085 ± 0.0194, equivalent to a Br mass of 31.1 ± 2.2 ng. It can be noted that the values obtained with or without outliers do not differ significantly from the theoretical value of 30 ng (Student's t-test, $t_{exp} = 0.676 < t_{crit}95\% = 2.228$, n=11; $t_{exp} = 1.500 < t_{crit}95\% = 2.306$, n=9). Moreover, there is no significant difference between the mean results obtained in both cases (Student's t-test, $t_{exp} = 1.232 < t_{crit}95\% = 2.145$, degrees of freedom = 14, two tails, different variance), but a much better precision

is achieved if these two values are rejected (Fisher's test, $F_{exp} = 6.025 > F_{crit95\%} = 4.295$, two tails).

Overall, removing outliers is possible with both approaches but it is important to emphasize that they are not going to influence MEC and MER results to the same degree. In any case, robust statistical approaches that are less affected by the occurrence of outliers are available both for performing regressions and for calculating the most representative value of a group of data, but it is out of the scope of this paper to further discuss such topic.

Both strategies, MEC and MER, represent different ways to extract analytical information from the same set of data and their distinct behavior will be further investigated in this work.

3.2. Monitoring CaBr around 625 nm: different intensity transitions

As discussed in section 3.1.1., there is an analytical limitation when low- or high-value slopes are used for MEC and, due to the similarity of the equations, MER should be influenced by these extreme values as well. Therefore, it is important to verify this behavior experimentally.

The first experiment consisted in evaluating the RSD obtained for the final Br concentration by measuring a blank solution, in order to subtract its values at each studied wavelength (pixel), and ten different Br masses: 10, 20, 30, 40, 50, 60, 80, 100, 120 and 150 ng (10 μL of standard solutions diluted accordingly). All measurements were done in triplicate. The data was treated as follows: assuming 10 ng Br is the sample, thus 20 ng Br could be treated as 10 ng Br sample +10 ng Br spike. This is equivalent of using MEC or MER with a theoretical value S = R = 0.5. Moreover, 20 ng Br could be treated as a sample and compared with 30 ng Br (10 ng Br spike), with a theoretical S and R of 0.667, and so forth. All the

possible combinations were evaluated for both MEC and MER and the results are shown in **Figure 4**. The slope and ratio axes use logarithm scale for better visualization of lower values. In **Figure 4B** a column goes out of scale, with an RSD of 117% (sample Br mass 50 ng with R = 0.833), but the maximum of the z-axis was set at 50% in order to use the same axis for both Figures 4A and 4B, thus enabling an immediate comparison.

Both strategies show a similar behavior: for all the Br mass studied, there is an increase in the final RSD at higher slope or ratio values. This fact agrees well with the theoretical values discussed previously for MEC (see **Figure 2**). A quite constant value of RSD through all the slope and ratios was obtained for 10 ng of Br because for low slope or ratio values only slight variations are found (as discussed before, the content of the sample hardly influences the signal). The RSDs are generally higher for low sample Br masses due to their proximity to the limits of detection (LOD). The transitions with lower intensities are more prone to be influenced by the instrumental noise and/or baseline fitting, which increase the uncertainty of the measurement at low Br masses.

It is also clear that the RSD is usually higher for MER than for MEC. MER weighs all the ratios equally, thus it is more sensitive to suffer from outliers, if no values are excluded. However, MER also provides an intuitive way to understand all the potential issues, as shown in **Figure 5**. **Figure 5A** shows the results for a Br mass of 30 ng in a sample with different spikes (10, 20, 30, 50, 70, 90 and 120 ng Br), and it plots the Br mass finally obtained using MEC *versus* the slope calculated experimentally. In this example, as predicted, the use of lower slopes results in lower RSDs (error bars show the standard deviation). However, such low slopes are also accompanied by a higher deviation from the true value. This

effect was commented in Section 3.1.1., that lower slopes/ratios values could lead to poorer accuracy due to the non-optimal relation between sample and spike. The same effect is observed in other strategies such as standard addition and isotope dilution, where it is well-known that the relation between spike and sample contents should be close to one, if possible.

For MER, a similar trend can be seen for the ratios: use of higher values lead to higher uncertainties, (see the small graph inside **Figure 5B**). However, if each individual value (the ratio of each transition) is plotted (see **Figure 5B**), it is possible to visualize a zone with a high-density of similar ratios (similar Br mass). If only those values are selected, the final results will be closer to MEC results. Moreover, observing R = 0.6, the Br mass is 35.2 ± 18.3 ng considering all the data. Obviously, there is an outlier with a value of approximately 85 ng, 2.5 times higher than the average and exceeding the average value plus 2 standard deviations. Eliminating this data with a Dixon's Q test (Q_{exp} = 0.825 > $Q_{crit95\%}$ = 0.466, n=10), the final value changes to 29.5 ± 3.6 ng, which obviously represents much better accuracy and precision. As discussed before, we do not want to complicate too much this topic and to carry out any unfair comparison, but simpler robust estimators (use of median and quartiles; use of the trimmed mean and the robust standard deviation) could and probably should be used for MER instead of relying on tests to reject outliers.

In conclusion, while Virgilio *et al.* recommended using slope values between 0.1 and 0.9 for MIP OES, ICP OES and ICP-MS,[24] it seems advisable to limit this range more and use values between 0.5 and 0.6 in the case of monitoring CaBr using HR CS GFMAS for both MEC and MER strategies to guarantee a well-balanced relation between accuracy and precision.

3.3. Effect of analyte-mass linearity for MEC and MER. Figures of merit

It is already well-known that AAS and MAS measurements obey the Lambert-Beer Law, but only for a relatively narrow range of masses. A linear relation between the analytical signal and the analyte mass can be established for one, or maximum two orders of magnitude. It is already well-established what this concept means when external calibration is deployed (*e.g.* need for diluting samples that provide a signal outside the linear range): However, it is necessary to also discuss what this fact represents when trying to use MEC or MER.

Figure 6 shows the response of the HR CS GFMAS instrument (integrated absorbance) for several masses of Br, between 20 and 400 ng (n=8), monitoring CaBr molecule, at the 11 transitions evaluated in the previous sections around 625 nm. The calibration curves for the most sensitive transitions show linearity until approximately 120 ng (other experiments show that 150 ng is still a safe value) and they lose linearity for a higher Br mass. Less sensitive transitions seem to show linearity in other ranges,[33] from 120 or 200 to 400 ng and probably more, but notice that such linearities (*e.g.*, from 200 to 400 for pixels 131, 114 and 100) do not necessarily go through the intercept. That means that this second range of linearity could be used for external calibration,[35] but not for MEC or MER as the equations shown in sections 3.1.1 and 3.1.2 will not be valid.

It is thus important to stress that lack of linearity may affect the determination of the analyte concentration by MEC and MER. Both methods rely on a linear and constant relation between the analyte and the instrumental signal regardless of the amount, *i.e.*, if one of the contents falls outside of the linear range, the calculations should be incorrect, as both contents (sample, and sample plus standard) will obey to different analyte *vs*. mass relations. The fact that the

linear range may be different for different transitions may be taken into account when designing the experiments, and eventually may minimize the number of transitions that should be used for a particular analyte amount.

Another limitation for using some lines depending on the analyte amount is the limit of quantification (LOQ). The traditional method for calculating LOD and LOQ is three and ten times the standard deviation (SD) of ten measurements of blank divided by the calibration curve slope, respectively. Using this approach, the LOD and LOQ of each wavelength (pixel) previously studied were calculated and the results are shown in **Table 3**, labelled as external calibration (EC). The LOD of pixel 168 which corresponds to the wavelength 625.315 nm, the usual analytical line studied for Br determination *via* CaBr molecule, was 3 ng, comparable to the values found in the literature for such transition (between 2.0 and 5.4 ng),[33,36,37] all higher than the value of 78 pg achieved by Limburg & Einax.[38]

LOD and LOQ definitions can also be applied in combination with the MER strategy. A blank signal plus $3SD_{10blank}$ or $10SD_{10blank}$ is considered as the signal of the sample, and equation 11 is used to calculate R for each transition and each spike used. Then equation 12 is applied to estimate the LODs and LOQs. These values are also shown in **Table 3**. Three Br spikes were chosen for this purpose: 20, 80 and 150 ng

Calculating the LOD and LOQ for MEC is, however, not equally straightforward. It requires the calculation of the slope through linear regression, comparing two analytical signals, sample and sample+standard, to later apply equation 5. In this case, the “sample” is the blank solution that by definition is the absence of analyte, *i.e.*, there is practically no analytical signal under normal

conditions. In the x-axis, intensity values proportional to the sensitivity of each transition due to the spike (blank+standard) will be plotted, while the y-axis should provide almost random intensity values due to the blank. Therefore, a linear correlation cannot be expected (see **Figure S1**).

Very recently, Virgilio *et al.* have proposed a method for calculating LOD/LOQ for multi-signal calibrations, including MEC.[24] The authors use equation 13 to calculate the LOD/LOQ, where S_{Slope} is the standard deviation of the MEC slope, and N is 3 when calculating the LOD, and 10 for the LOQ. Thus, this strategy was also investigated, and the results are shown in **Table 4**.

$$LOD\ or\ LOQ = N\left(\frac{C^{Std}S_{Slope}}{(1-Slope)^2}\right) \qquad (13)$$

Four different strategies were evaluated with this approach. Calculation by: i) using the 11 transitions around 625 nm (see **Table 2**); ii) using the three most sensitive transitions (pixels 131, 149 and 168); iii) using the same 11 pixels as in i), but considering Slope = 0; and iv) using the same 3 pixels as in ii), but considering Slope = 0. The first strategy is similar to the one proposed by Virgilio *et al.*[24] The second uses equation 13 with the minimum number of different transitions recommended for a MEC analysis, which is three, as discussed by Donati & Amais.[3] The third and fourth ones are estimations based on the following concept. As discussed before, MEC should compare two analytical signals, but in this case, one corresponds to a blank solution that shows a random behavior. Thus, the data plotted would hardly follow any linear tendency (see **Figure S1** for examples). It is not evident that the slope resulting from such calculation would possess any physical meaning. Therefore, we assume that a theoretical perfect

blank should result in a slope value of zero, and the estimation of LOD/LOQ should only account for the uncertainty of the slope measurement.

As shown in **Table 3**, the LODs and LOQs calculated for MER 80 and MER 150 are, for the most sensitive wavelengths, comparable to those obtained using EC. This can be explained because using the method described for calculating the LOD/LOQ for MER is analogue to using a one-point calibration curve, which would be the spike, since the signal from the blank solution should be negligible in comparison with the signal of the spike. Following the same argument, MER 20 probably has a bit “higher slope” (linearity is never perfect), leading to lower values of LOD/LOQ.

MER 150 shows lower LOD/LOQ values at low-sensitive wavelengths than MER 80. That could have been expected, as higher analytical signals should be less affected by random events. Moreover, comparing the previous strategies for the most sensitive transitions (**Table 3**, pixel 168) with the LOD/LOQ calculated with equation 13 for MEC using first and third strategies, both making use of 11 transitions (see **Table 4**), they are all rather similar.

In any case, we believe that calculating LODs and LOQs using the MER approach is always useful to assess which lines should be considered and which rejected as a function of the analyte content. On the other hand, when providing the overall figure of merit, a method should not have various limits, and a suitable strategy to calculate the global LOD and LOQ should be proposed for MER. As mentioned above, Donati & Amais[3] stated that at least three transitions are needed to use MEC, and in this case we will follow the same criteria for MER. Therefore, it is reasonable that the three most sensitive analytical lines should be considered for calculating the overall LOD/LOQ.

Pixel 131 (λ = 625.128 nm) measures the third most sensitive transition in this region, with a relative sensitivity of 58% compared with the highest peak (625.315 nm). However, during the analysis, an unidentified molecule (see **Figure 7**) was observed when only the blank solution was monitored with both chemical modifier (Pd) and molecule-forming reagent (Ca). This molecule was generated only when the graphite furnace was new and calcium was used. Due to the refractory nature of this molecule (wide-time profile and low intensity), it could be a calcium oxide polyatomic molecule, which has been reported to show a transition at 625.85 nm.[39] The interfering molecule could not be eliminated with background least-square correction, available from the AspectCS software, and it especially hampers the measurement at 625.128 nm. Integrating the first 2 s of signal only minimizes the effect of this overlap for the CaBr analytical signal, an approach that was used throughout this study whenever this interfering molecule was detected. Moreover, it is visible that the baseline in this region (see **Figure 7**) shows a "wavy" profile, which may also influence the determination of peak relations, especially the ones with low intensity. Overall, pixel 114 (λ = 625.045 nm) was used as the third most sensitive line for the current method instead of pixel 131 (λ = 625.128 nm).

Obviously, the overall limits are finally restricted by the highest LOD/LOQ values of the three, *i.e.*, pixel 114 at 625.045 nm. Consequently, in this case we propose a LOD and LOQ of 6 ng and 21 ng, respectively, for the MER strategy. Both figures of merit can be calculated directly as explained without needing any external standard calibration to obtain this value. Nevertheless, using lower amount of spike could be a strategy to improve a bit the LOD and LOQ.

Using the same hypothesis for equation 13 (use of the 3 most sensitive transitions only), the values varied from 10 and 33 to 14 and 48 for LOD and LOQ, respectively (see **Table 4**). Assuming a slope value of blank as zero, the limits are practically identical, as the slope is very low in comparison with 1.

In principle, as mentioned by Virgilio *et al.*[24] these multi-signal methods will typically show higher values of LOD/LOQ compared to external standard calibration all things considered, as for EC only the most sensitive line is used and for these approaches more, less sensitive and more noisy lines need to be used. However, the difference between MEC and MER here is that, at least applying the equations proposed in ref. 24, MEC benefits from the use of more transitions as lower LODs and LOQs are provided then (see **Table 4**). This is a bit paradoxical, as those extra transitions added offer poorer sensitivity.

Overall, we would recommend simply using MER for calculating the LODs and LOQs of the lines tested, as such approach provides useful information for selecting the most suitable ones according to the sample concentration. Such criteria will be used in the next sections to select the lines for the determinations intended.

3.4. Monitoring CaBr around 600 nm: similar intensity transitions

Considering the results shown in section 3.2., MEC could be considered as a bit more suitable as calibration strategy for CaBr molecule detection using HR CS GFMAS around 625 nm mainly because it leads to lower RSD values. The mean value of Br mass obtained by both MEC and MER are similar, and for both strategies is advisable to work in the vicinity of S = R = 0.5.

However, the vibronic transition studied in that section, $X^2\Sigma \rightarrow A^2\Pi$ (0,0),[39] shows an interesting profile where lines with increasing intensities appear. This

is not always the case. For other molecules monitored by HR CS MAS for the determination of non-metals (*e.g.*, CS, widely proposed to determine S,[17,28,40] or PO, used to determine P[17,28,41]) this behavior is not encountered, but instead many lines of similar sensitivity are measured.[42] Interestingly, this other type of profile can also be investigated measuring CaBr as well. There is another vibronic transition for the CaBr molecule, $X^2\Sigma \rightarrow B^2\Sigma$ (1,0), which appears around 600.24 nm and has been previously explored for isotopic analysis.[43] In this region, all the transitions of CaBr show similar intensities when Br is found in the natural composition (50.7% ^{79}Br and 49.3% ^{81}Br), except for two larger peaks at 600.321 and 600.426 nm where there is an overlap from the transitions of Ca^{79}Br and Ca^{81}Br (thus, practically a double signal is measured; see **Figure 1B** where these overlapped lines are labelled in red). Therefore, this region was studied with MEC and MER to evaluate their performance in this context.

Seventeen peaks were selected between 600.115 and 600.835 nm (all the pixels but the two larger ones; see **Figure 1B**). The temperature and chemical modifiers are the same listed in **Table 1**, and the results are displayed in **Figure 8**.

The small differences on the peak intensities reveal a major effect on the signal relations in MEC (see **Figure 8A**), which was already observed for CS, PO and NO molecules using HR CS MAS with flame as atomizer, as several transitions needed to be excluded to improve the linearity.[17] Overall, there is a linear tendency, r^2 = 0.9583, but not all the points follow well the trend, and visually there is no easy criteria to select which outliers could be removed. The problem is that all those points in practice behave like three or four different groups of points, instead of like a high number of points more or less evenly

distributed along the line, like in **Figure 3A**. In this case, the theoretical slope and ratio is 0.5. The slope obtained (0.5725 ± 0.0350) resulted in a Br mass of 134 ± 19 ng, which is 34% biased high. If we include in the regression both pixels 59 and 84 (600.321 and 600.426 nm, respectively, red-labelled peaks in **Figure 1B**) that show more sensitivity (lines for which $Ca^{79}Br$ and $Ca^{81}Br$ signals overlap), the MEC slope approximates better to the true value as 0.5364 ± 0.0220 (116 ± 10 ng Br) is obtained, further supporting the concept that the MEC approach benefits from a higher sensitivity variation between lines (see **Figure 8B**).

When the MER approach is followed (see **Figure 8C**), the small difference between line sensitivities does not appear to show any clear influence for this strategy, as could be expected. Using more ratios provides a more robust estimation. The ratio estimated, 0.5234 ± 0.0313, is converted to 110 ± 14 ng Br, with a bias of 10%, which is in any case within the precision of the measurements.

In conclusion, it is possible to assume that MEC could be usually recommended as a calibration strategy, unless the available transitions show similar sensitivities, a situation where MER should be considered instead.

3.5. Non-spectral interference

As discussed before, both strategies show higher limits of detection compared to external standard calibration, but they can help in detecting the occurrence of spectral overlaps at distinct transitions, which should result in outliers. Moreover, MEC and MER show potential to correct for matrix effects with only two solutions, in a similar way as what occurs with isotopic dilution,[43,44] or with standard addition (even though for the latter more points are usually prepared and measured to minimize the uncertainty of the final results when extrapolating).

A common problem in the case of HR CS MAS is the occurrence of interferences due to chemical competition with other species present in the matrix, affecting the formation of the target species. In the case of monitoring the diatomic molecule CaBr, there are two possibilities: the presence of species that interact with Br, not leaving it available to Ca (*e.g.,* Al) or the presence of species that react with Ca (*e.g.,* other halogens), which would eventually lead to the same effect: formation of less CaBr.[43]

One of the elements more commonly present in a sample at sufficiently high levels to compromise the formation of the CaBr diatomic molecule is Cl. Nakadi *et al.*[43] already studied the interference of chlorine on the determination of Br *via* the monitoring of the CaBr molecule by HR CS GFMAS. In that work, the presence of Cl resulted in 80% of sensitivity loss for the signal of CaBr when it was found at an amount (in moles) 10 times higher than Br. The problem was circumvented using isotopic dilution as calibration strategy, a powerful approach, but one that requires looking for alternative, less sensitive transitions that show sufficiently high isotopic shifts, besides the use of an isotopic spike.

Under these circumstances, use of MEC and MER could be a more general way to compensate for this effect, because the change in the analytical signal caused by the presence of Cl should be proportionally the same in the sample and in the sample plus the spike, and thus the slope/ratio should be constant.

To evaluate this hypothesis, a 30 ng standard solution of Br was used as sample and CaBr was monitored around 625 nm. Four Br spikes were studied (10, 20, 30 and 40 ng Br) with three different Cl spikes: 0, 500 and 1000 ng of Cl as sodium chloride. Both MEC and MER were compared for each set of data,

and the results are shown in **Figure 9**. Four pixels were used for this study (both MEC and MER), namely 114, 131, 149 and 168, due to their figures of merit, as the rest of the pixels did not provide a LOQ ≤ 30 ng (see **Table 3**).

Evaluating pixel 168 (λ = 625.308 nm), there was a 35% decrease in the CaBr analytical signal when 500 ng Cl were added, and 54% for 1000 ng Cl. Nonetheless, using MEC (blue bars) and MER (yellow bars) it is possible to circumvent this interference, as can be seen in **Figure 9**. It is noteworthy that, as described previously, working at a slope/ratio around 0.5 usually leads to better accuracy (difference with the true value lower than 8% considering all Cl masses) Opting for a lower slope/ratio (0.4), results biased high seem to be obtained, while for a slope/ratio of 0.75 the results are a bit biased low. In this case, using four transitions only produces increased RSD values for MEC in comparison with MER, as could be appreciated in the error bars of **Figure 9**.

Overall, both strategies were successful in correcting for the Cl interference in this study. Nevertheless, it seems advisable to carry out a previous study to have an approximate idea of the sample content before spiking it, or either to test various spikes to finally work with that providing a slope/ratio close to 0.5 - 0.6.

3.6. Determination of Br in water sample using MEC and MER

A CRM water (QC3060) was used to evaluate how both strategies can correct for the occurrence of interferences and validate the method in a complex matrix. This CRM provides the concentration of bromide (2.81 ± 0.42 mg L^{-1}) in addition of several anions, such as the halogens chloride (54.9 ± 8.2 mg L^{-1}) and fluoride (2.52 ± 0.38 mg L^{-1}), and others with higher concentrations as nitrate (66.1 ± 9.9 mg L^{-1}) and sulfate (81.5 ± 12.2 mg L^{-1}). Five transitions were

evaluated (pixels 100, 114, 131, 149 and 168) around 625 nm, pipetting 20 μL of the sample (56.2 ± 8.4 ng Br) instead of 10 μL to increase the signal, with three Br spikes of 20.4, 58.3 and 96.6 ng. The results obtained are listed in **Table 5**.

Using external standard calibration (calibration range 20 – 100 Br ng, 5 points, r^2 = 0.9993, λ = 625.315 nm), the Br concentration was calculated to be 0.282 ± 0.022 mg L^{-1}, which represents only around 10% of recovery, further highlighting the influence of the concomitant species. As predicted, using a slope/ratio close to 0.5 leads to better values with both MEC and MER, with RSDs of 15% and 8%, and a deviation of the average value of only 5.6% and 1.5%, respectively, well within the uncertainty of the measurements.

In any case, all the conditions evaluated lead to results that overlap with the expected value. However, for a 0.75 slope/ratio value, the uncertainty remains higher than the others (in particular for MEC), demonstrating that high slopes should be avoided. Despite this high uncertainty at 0.75, use of MEC provides practically the same average value for all the spikes, proving its robustness.

MEC was also evaluated with conventional least-squares regression (MEC_Y) for further comparison. Both MEC strategies lead to similar average results, although the uncertainty is larger when using York method (see 3.1.1.), as expected, because the error sources from both axes are considered in such case. Such difference becomes more relevant when using high S values (S ≅ 0.75).

Overall, all strategies, when properly optimized, enable circumventing these non-spectral interferences caused by competing species, supporting their use as a valuable alternative method of calibration when performing HR CS GFMAS.

4. Conclusions

The limitations and application of the MEC calibration strategy for determining non-metals *via* HR CS GFMAS was verified in this study, using CaBr as a proxy. Moreover, another similar approach that only differs in the way in which the data is processed (MER) was proposed and evaluated as well for the first time, comparing its performance with that of MEC in different circumstances.

This work confirms previous reports indicating that MEC is a useful tool as a calibration alternative due to its advantage of needing only the preparation and measurement of two aliquots (sample, and sample plus spike) to determine the analyte concentration. Furthermore, this study presents some new conclusions for the best use of both MEC and MER: i) use of too high or too low slope/ratios is not recommended, and values between 0.5 and 0.6 should be chosen; ii) MEC could provide better precision, but its use is favored when many transitions of dissimilar sensitivity are available; if, on the other hand, the transitions available are only a few or show similar sensitivities, the use of MER can provide better results. Furthermore, the calculation of LODs and LOQs using MER is proposed, as it enables checking which lines are above these limits for any particular determination. In any case, it should always be remembered that both the analyte contents of the sample and of the sample plus standard should fall within the working linear range for all the lines considered.

The measurements were hampered mainly by the wavy baseline and occasional appearance of an unknown molecule, as well as by the occurrence of chemical interferences that prevented the quantitative formation of CaBr. Nevertheless, accurate results could be obtained for both MEC and MER, under optimal conditions, proving that these can be very valuable analytical tools for HR

CS GFMAS. Moreover, this conclusion can be expanded to other techniques that are prone to be affected by similar issues, and where several different analytical signals can be derived from a single analyte.

Conflicts of interest

There are no conflicts of interest to declare

Acknowledgements

The authors are grateful to project PGC2018-093753-B-I00 (MCIU/AEI//FEDER, UE), to the European Regional Development Fund for financial support through the Interreg POCTEFA 176/16/DBS, and to the Aragon Government (Construyendo Europa desde Aragón). Raúl Garde acknowledges his predoctoral grant BES-2016-078971 (associated to project CTQ2015-64684-P) from the Ministerio español de Ciencia, Innovación y Universidades.

References

1. B. V. L'Vov, *J. Anal. At. Spectrom.*, 1988, **3**, 9–12.
2. A. Hulanicki, *Anal. Proc.*, 1992, **29**, 512–516.
3. G. L. Donati and R. S. Amais, *J. Anal. At. Spectrom.*, 2019, **34**, 2353-2369.
4. J. A. Carter, A. I. Barros, J. A. Nóbrega and G. L. Donati, *Front. Chem.*, 2018, **6**, 504.
5. P. Kościelniak and J. Kozak, *Crit. Rev. Anal. Chem.*, 2006, **36**, 27–40.
6. J. E. T. Andersen, *TrAC - Trends Anal. Chem.*, 2017, **89**, 21–33.
7. F. Vanhaecke, L. Balcaen and D. Malinovsky, *J. Anal. At. Spectrom.*, 2009, **24**, 863–886.
8. P. Rodríguez-González, J. M. Marchante-Gayón, J. I. García Alonso and A. Sanz-Medel, *Spectrochim. Acta, Part B,* 2005, **60**, 151–207.
9. K. G. Heumann, S. M. Gallus, G. Rädlinger and J. Vogl, *J. Anal. At. Spectrom.*, 1998, **13**, 1001–1008.
10. A. Virgilio, D. A. Gonçalves, T. McSweeney, J. A. Gomes Neto, J. A. Nóbrega and G. L. Donati, Anal. Chim. Acta, 2017, **982**, 31-36.
11. R. C. Machado, A. B. S. Silva, G. L. Donati and A. R. A. Nogueira, *J. Anal. At. Spectrom.*, 2018, **33**, 1168–1172.
12. D. V. Babos, A. Virgilio, V. C. Costa, G. L. Donati and E. R. Pereira-Filho, *J. Anal. At. Spectrom.*, 2018, **33**, 1753–1762.
13. A. S. Augusto, J. P. Castro, M. A. Sperança and E. R. Pereira-Filho, *J. Braz. Chem. Soc.*, 2019, **30**, 804–812.
14. D. F. Andrade, F. M. Fortunato and E. R. Pereira-Filho, *Anal. Chim. Acta*, 2019, **1061**, 42–49.

15. F. M. Fortunato, T. A. Catelani, M. S. Pomares-Alfonso and E. R. Pereira-Filho, *Anal. Sci.*, 2019, **35**, 165–168.
16. A. A. C. Carvalho, L. A. Cozer, M. S. Luz, L. C. Nunes, F. R. P. Rocha and C. S. Nomura, *J. Anal. At. Spectrom.*, 2019, **34**, 1701–1707.
17. A. L. Vieira, D. A. Gonçalves, A. Virgilio, E. C. Ferreira, B. T. Jones, G. L. Donati and J. A. Gomes Neto, *J. Anal. At. Spectrom.*, 2019, **34**, 972–978.
18. M. C. Alencar, D. A. Gonçalves, G. Nicolodelli, S. L. Oliveira, G. L. Donati and A. R. L. Caires, *Spectrochim. Acta, Part A*, 2019, 117221.
19. A. Virgilio, J. A. Nóbrega and G. L. Donati, *Anal. Bioanal. Chem.*, 2018, **410**, 1157–1162.
20. J. M. de Higuera, A. B. S. da Silva, A. F. de Oliveira and A. R. de Araujo Nogueira, *Food Chem.*, 2020, **303**, 125395.
21. E. Bolea-Fernandez, L. Balcaen, M. Resano and F. Vanhaecke, *J. Anal. At. Spectrom.*, 2017, **32**, 1660–1679.
22. L. Balcaen, E. Bolea-Fernandez, M. Resano and F. Vanhaecke, *Anal. Chim. Acta*, 2015, **894**, 7–19.
23. C. B. Williams and G. L. Donati, *J. Anal. At. Spectrom.*, 2018, **33**, 762-767.
24. A. Virgílio, A. B. S. Silva, A. R. A. Nogueira, J. A. Nobrega and G. L. Donati, *J. Anal. At. Spectrom.*, 2020, **35**, 1614-1620.
25. B. Welz, H. Becker-Ross, S. Florek and U. Heitmann, High-resolution Continuum Source AAS. The Better Way to Do Atomic Absorption Spectrometry, Wiley-VCH, Weinheim, 2005.
26. M. Resano, M. Aramendía and M. A. Belarra, *J Anal Spectrom*, 2014, **29**, 2229–2250.
27. M. Resano, E. García-Ruiz, M. Aramendía and M. A. Belarra, *J. Anal. At. Spectrom.*, 2019, **34**, 59–80.
28. M. Resano, M. Aramendía, F. V. Nakadi, E. García-Ruiz, C. Alvarez-Llamas, N. Bordel, J. Pisonero, E. Bolea-Fernández, T. Liu and F. Vanhaecke, *TrAC Trends Anal. Chem.*, 2020, **129**, 115955.
29. M. Resano, L. Rello, M. Flórez and M. A. Belarra, *Spectrochim. Acta, Part B,* 2011, **66**, 321–328.
30. M. Resano, M. R. Flórez and E. García-Ruiz, *Spectrochim. Acta, Part B,* 2013, **88**, 85–97.
31. B. Welz, F. G. Lepri, R. G. O. Araujo, S. L. C. Ferreira, M. D. Huang, M. Okruss and H. Becker-Ross, *Anal. Chim. Acta*, 2009, **647**, 137–148.
32. M. Resano, M. R. Flórez and E. García-Ruiz, *Anal. Bioanal. Chem.*, 2014, **406**, 2239–2259.
33. M. R. Flórez and M. Resano, *Spectrochim. Acta, Part B,* 2013, **88**, 32–39.
34. https://www.originlab.com/doc/Origin-Help/LinearFit-XErr-Dialog, accessed in 2020, July 14th
35. B. Welz, L. M. G. dos Santos, R. G. O. Araujo, S. do C. Jacob, M. G. R. Vale, M. Okruss and H. Becker-Ross, *Spectrochim. Acta, Part B,* 2010, **65**, 258–262.
36. M. D. Huang, H. Becker-Ross, S. Florek, U. Heitmann and M. Okruss, *Spectrochim. Acta, Part B,* 2008, **63**, 566–570.
37. É. R. Pereira, I. N. B. Castilho, B. Welz, J. S. Gois, D. L. G. Borges, E. Carasek and J. B. De Andrade, *Spectrochim. Acta, Part B,* 2014, **96**, 33–39.
38. T. Limburg and J. W. Einax, *Microchem. J.*, 2013, **107**, 31–36.
39. R. W. B. Pearse and A. G. Gaydon, The Identification of Molecular Spectra, fourth ed., Chapman and Hall Ltd., London, 1976.
40. N. Ozbek and A. Baysal, *TrAC - Trends Anal. Chem.*, 2017, **88**, 62–76.

41. L. C. Pomarolli, M. A. M. Silva da Veiga, M. Resano, F. V. Nakadi, *J. Anal. At. Spectrom.*, 2020, in press, 10.1039/d0ja00254b
42. D. J. Butcher, *Anal. Chim. Acta*, 2013, **804**, 1–15.
43. F. V Nakadi, M. A. M. S. da Veiga, M. Aramendía, E. García-Ruiz and M. Resano, *J Anal Spectrom*, 2016, **31**, 1381–1390.
44. F. V. Nakadi, M. A. M. S. da Veiga, M. Aramendía, E. García-Ruiz and M. Resano, *J Anal Spectrom*, 2015, **30**, 1531–1540.

Table 1. HR CS GFMAS conditions for the determination of Br *via* the monitoring of CaBr.

Vibronic transition / Central pixel wavelength	$X^2\Sigma \rightarrow A^2\Pi$ (0,0) / 624.997 nm
	$X^2\Sigma \rightarrow B^2\Sigma$ (1,0) / 600.492 nm
Number of detector pixels	5 (CP±2)
Sample volume / μL	10, 20*
Chemical modifier	Pd (30 μg)
Molecule-forming reagent	Ca (150 μg)

Temperature program

Step	**Temperature / °C**	**Ramp / °C s^{-1}**	**Hold / s**	**Ar gas flow / L min^{-1}**
Drying	90	5	20	2.0
Drying	120	5	30	2.0
Pyrolysis	1000	50	20	2.0
Gas adaption	1000	0	5	0.0
Vaporization	2100	3000	4-6**	0.0
Cleaning	2500	500	4	2.0

*used for the determination of Br in the CRM QC3060

** The signal is integrated during the first 2 seconds

Table 2. Relation between the detection pixel number and the wavelength for the vibronic transitions $X^2\Sigma \rightarrow A^2\Pi$ (0,0) and $X^2\Sigma \rightarrow B^2\Sigma$ (1,0) of the CaBr diatomic molecule.

Transition $X^2\Sigma \rightarrow A^2\Pi$ (0,0)		**Transition $X^2\Sigma \rightarrow B^2\Sigma$ (1,0)**	
Pixel	**Wavelength / nm**	**Pixel**	**Wavelength / nm**
40	624.685	11	600.115
46	624.714	20	600.153
54	624.753	44	600.253
63	624.797	51	600.283
74	624.850	59*	600.321
86	624.909	68	600.354
100	624.972	74	600.379
114	625.045	84*	600.426
131	625.128	94	600.463
149	625.211	100	600.488
168	625.315	109	600.526
		122	600.580
		127	600.601
		136	600.639
		143	600.668
		151	600.701
		165	600.760
		175	600.802
		183	600.835

*Overlapped peaks

Table 3. Figures of merit corresponding to the CaBr vibronic transition $X^2\Sigma - A^2\Pi$ (0,0) using HR CS GFMAS. External calibration (the calibration curve covered a Br mass range between 10 and 150 ng) is labelled as EC. Each number besides MER corresponds to the Br mass spike, in ng, used for the calculation of LOD and LOQ. Both EC and MER were evaluated using 11 wavelengths (pixels). n.a.: not applied.

Pixel	LOD; LOQ / ng Br			
	EC	***MER 20***	***MER 80***	***MER 150***
40	40; 135	n.a.	86; 286	54; 181
46	52; 174	n.a.	116; 386	70; 235
54	43; 142	n.a.	89; 297	57; 189
63	53; 178	n.a.	143; 476	82; 274
74	22; 72	15; 50	25; 84	23; 77
86	26; 87	25; 84	34; 115	30; 100
100	17; 55	11; 36	18; 61	18; 59
114	6; 21	3; 10	6; 20	6; 21
131	9; 30	4; 15	9; 30	9; 30
149	4; 14	2; 6	4; 13	4; 14
168	3; 11	1; 4	3; 10	3; 10

Table 4. Figures of merit corresponding to the CaBr vibronic transition $X^2\Sigma - A^2\Pi$ (0,0) using HR CS GFMAS and MEC calculated *via* equation 13. N_T represents the number of transitions used for the calculation of the LOD/LOQ, and S is the theoretical value of slope.

Br spike / ng	LOD; LOQ / ng Br			
	$N_T = 11$	$N_T = 3$	$N_T = 11$, S = 0	$N_T = 3$, S = 0
20	3; 9	10; 33	3; 9	10; 32
80	3; 11	13; 43	3; 11	13; 43
150	4; 12	14; 48	4; 12	14; 48

Table 5. Determination of Br in QC3060 *via* the monitoring of CaBr with HR CS GFMAS using MEC and MER strategies. Uncertainties are given as 95% confidence intervals (n=5). n.a.: not applied. MEC values are obtained as recommended in this work (see 3.1.1.), while for MEC_Y, conventional linear regression considering only the errors in y-axis was used.

Br mass	**Slope/Ratio**			**Br concentration / mg L^{-1}**				
spike / ng	**MEC**	**MEC_Y**	**MER**	**MEC**	**MEC_Y**	**MER**	**EC**	**Reference**
0	n.a.	n.a.	n.a.	n.a.	n.a.	n.a.	0.282 ± 0.022	
20.4	0.745 ± 0.116	0.743 ± 0.054	0.716 ± 0.023	2.97 ± 2.10	2.94 ± 0.86	2.57 ± 0.36	n.a.	2.81 ± 0.42
58.3	0.504 ± 0.045	0.504 ± 0.039	0.495 ± 0.020	2.97 ± 0.54	2.96 ± 0.47	2.85 ± 0.29	n.a.	
96.6	0.390 ± 0.036	0.392 ± 0.033	0.376 ± 0.017	3.08 ± 0.47	3.11 ± 0.43	2.91 ± 0.27	n.a.	

Figure captions

Figure 1. Spectra of the CaBr diatomic molecule (A) in the vicinity of 625.0 nm, as obtained with 30 ng Br; and (B) in the vicinity of 600.5 nm, as obtained with 100 ng Br. The numbers over the peaks correspond to the detection pixel at a specific wavelength (see **Table 2**). Graphite furnace conditions are listed in **Table 1**.

Figure 2. Theoretical relation between different deviations from the true slope (1, 5 and 10%, with different shades of blue) and the final bias in the concentration calculated using MEC.

Figure 3. Experimental data (11 transitions) obtained for 30 ng Br as sample and 30 ng Br as spike using HR CS GFMAS for the monitoring of CaBr in the vicinity of 625 nm with (A) MEC and (B) MER strategies. Error bars correspond to the standard deviation (n=3). The labels shown in Figure 3A correspond to the pixels measured

Figure 4. Evaluation of the RSD of the Br masses calculated from standard solutions containing Br ranging 10 to 120 ng with different (A) slopes and (B) ratios using MEC and MER, respectively. In Figure 4B, the RSD value for sample Br mass 50 ng with 0.833 ratio is out of scale (actual value,117%).

Figure 5. Br determination (true mass 30 ng) through (A) MEC and (B) MER at different slopes/ratios. Each data of Figure 5B shows the mean value for each one of the transition evaluated. The small graph inside Figure 5B shows the overall mean value of all the transitions with its uncertainty. The red line corresponds to the real value (30 ng). The error bars correspond to the standard deviations (n=3).

Figure 6. Calibration curves (Br values ranging from 20 to 400 ng) when monitoring the CaBr molecule using HR CS GFMAS. The numbers of each calibration curve correspond to the detection pixels (wavelength) used to obtain the integrated absorbance (CP±2) of different rotational contributions of the vibronic transition $X^2\Sigma$ – $A^2\Pi$ (0,0). Error bars correspond to the standard deviation (n=3).

Figure 7. Time- and wavelength-resolved spectrum of the unknown molecular interference appearing in the analytical region around 625 nm.

Figure 8. Experimental data for 100 ng Br as sample and 100 ng Br as spike using HR CS GFMAS *via* monitoring of the CaBr molecule in the vicinity of 600 nm using: (A) MEC with 17 transitions; (B) MEC with 19 transitions (the 17 used before plus pixels 59 and 84); and (C) MER with 17 transitions. Error bars correspond to the standard deviation (n=3).

Figure 9. Study of the effect of the presence of Cl on the determination of Br *via* the monitoring of the CaBr molecule with HR CS GFMAS using MEC (blue bars) and MER (yellow bars) strategies for quantification. The gray surface indicates the real Br mass (30 ng). Error bars correspond to the standard deviation (n=5).

Figure 1

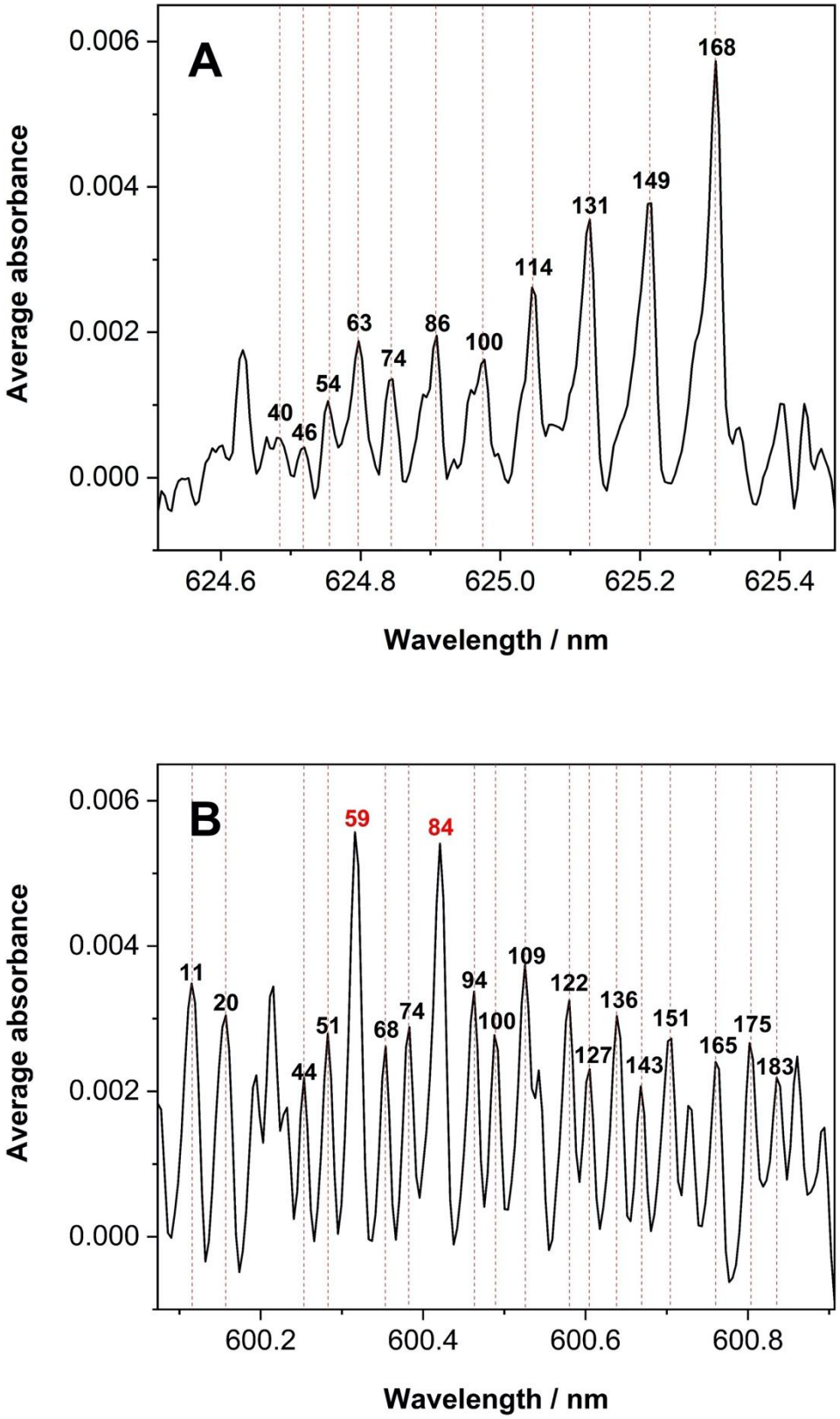
A
Average absorbance
0.006
0.004
0.002
0.000
40
46
54
63
74
86
100
114
131
149
168
624.6
624.8
625.0
625.2
625.4
Wavelength / nm
B
Average absorbance
0.006
0.004
0.002
0.000
11
20
44
51
59
68
74
84
94
100
109
122
127
136
143
151
165
175
183
600.2
600.4
600.6
600.8
Wavelength / nm

Figure 2

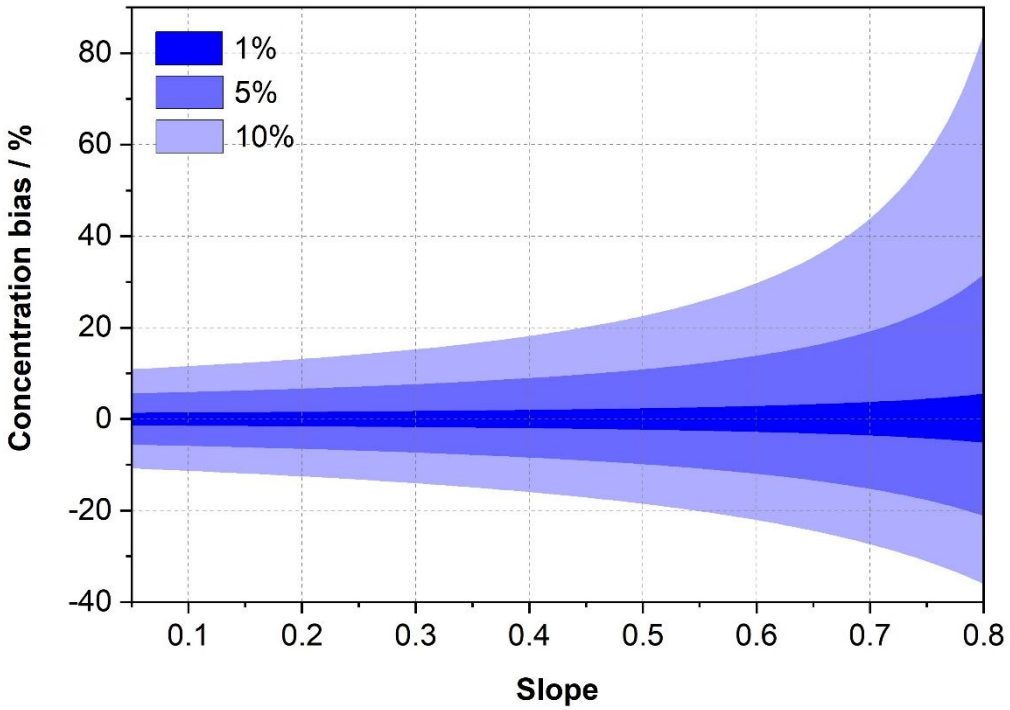
1%
5%
10%
Concentration bias / %
80
60
40
20
0
-20
-40
0.1
0.2
0.3
0.4
0.5
0.6
0.7
0.8
Slope

Figure 3

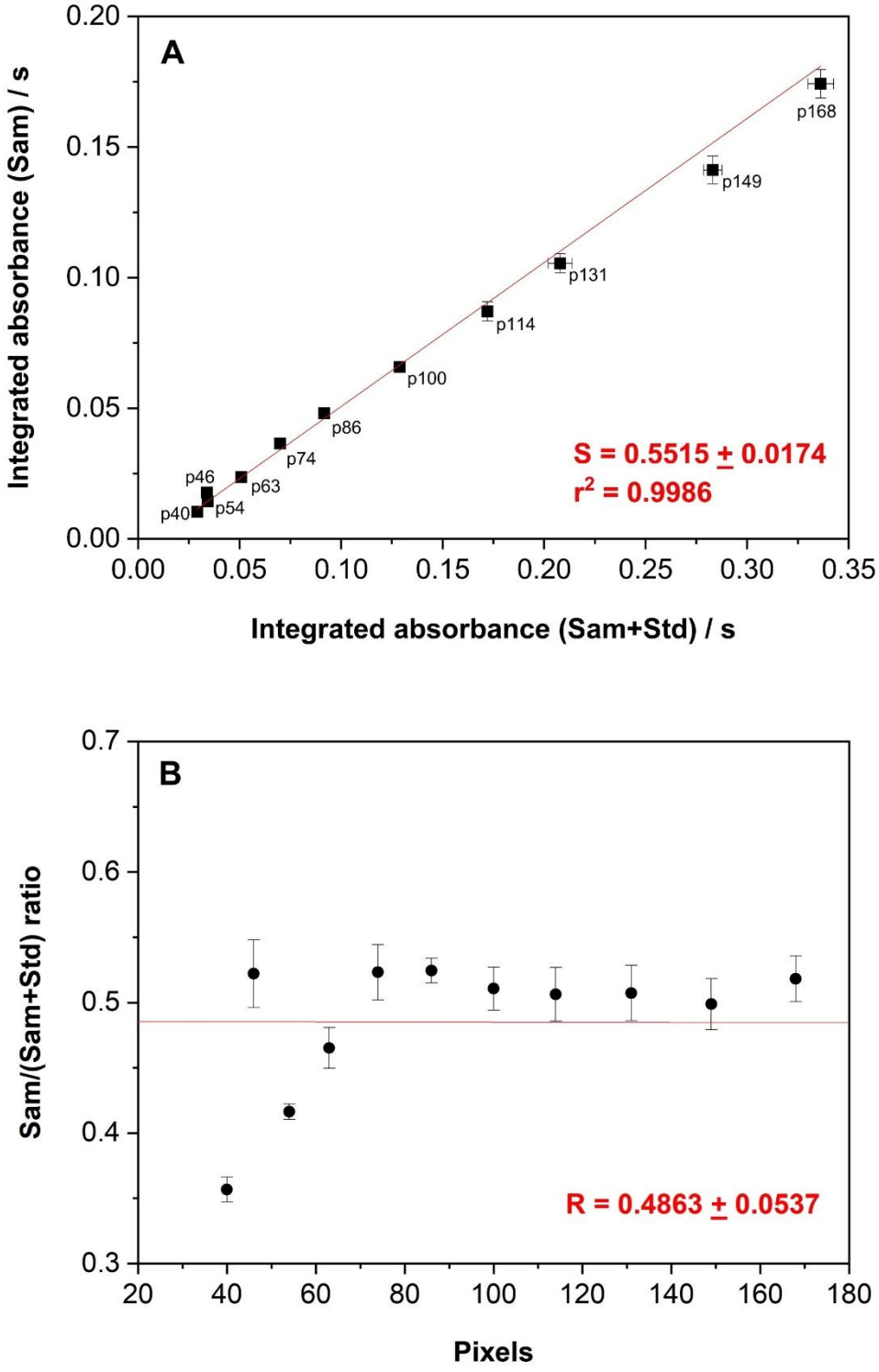
A
Integrated absorbance (Sam) / s
Integrated absorbance (Sam+Std) / s
0.00
0.05
0.10
0.15
0.20
0.25
0.30
0.35
p40
p46
p54
p63
p74
p86
p100
p114
p131
p149
p168
S = 0.5515 ± 0.0174
r2 = 0.9986
B
Sam/(Sam+Std) ratio
Pixels
0.3
0.4
0.5
0.6
0.7
20
40
60
80
100
120
140
160
180
R = 0.4863 ± 0.0537

Figure 4

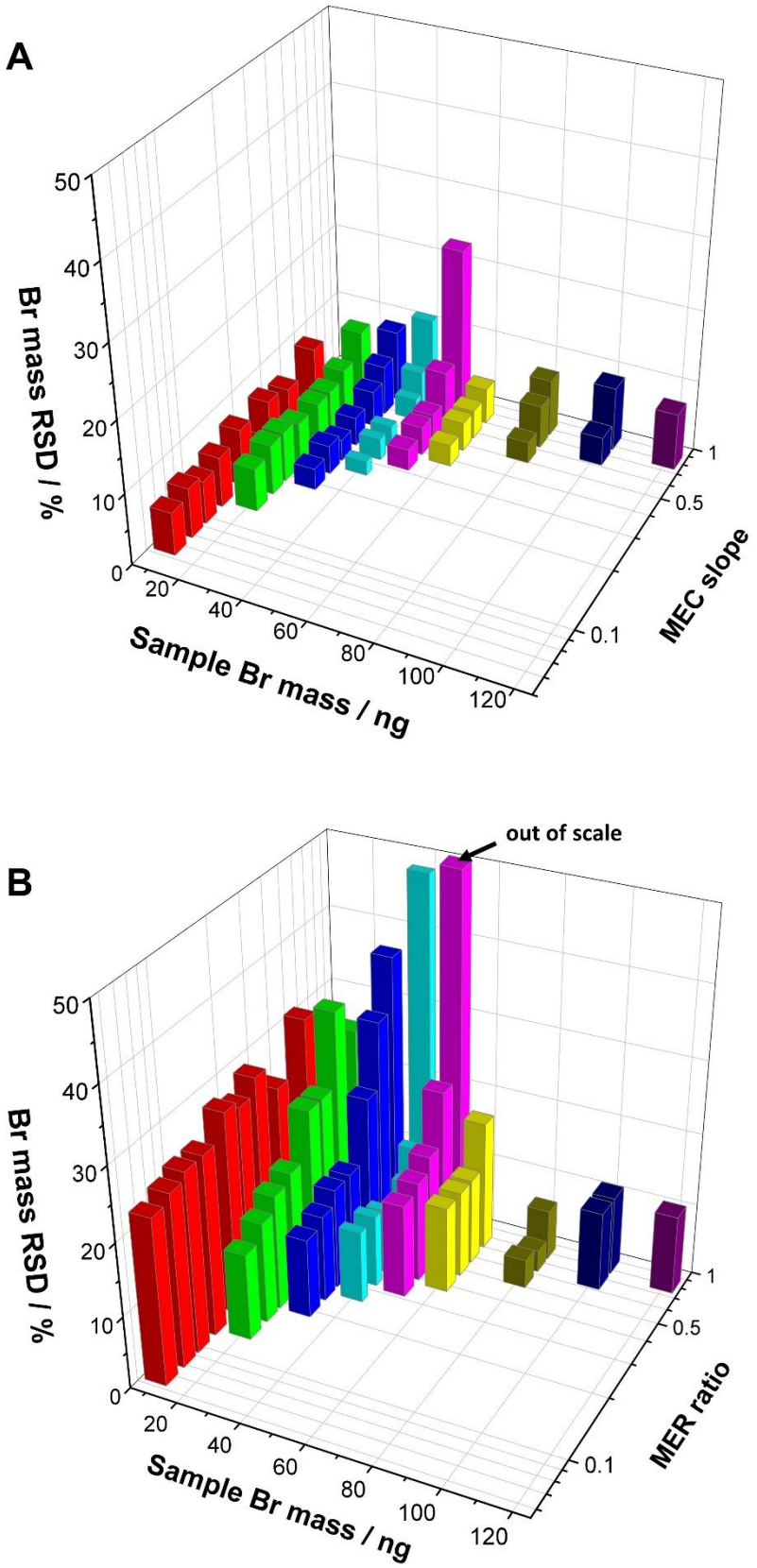
A
Br mass RSD / %
0
10
20
30
40
50
Sample Br mass / ng
20
40
60
80
100
120
MEC slope
0.1
0.5
1
B
out of scale
Br mass RSD / %
0
10
20
30
40
50
Sample Br mass / ng
20
40
60
80
100
120
MER ratio
0.1
0.5
1

Figure 5

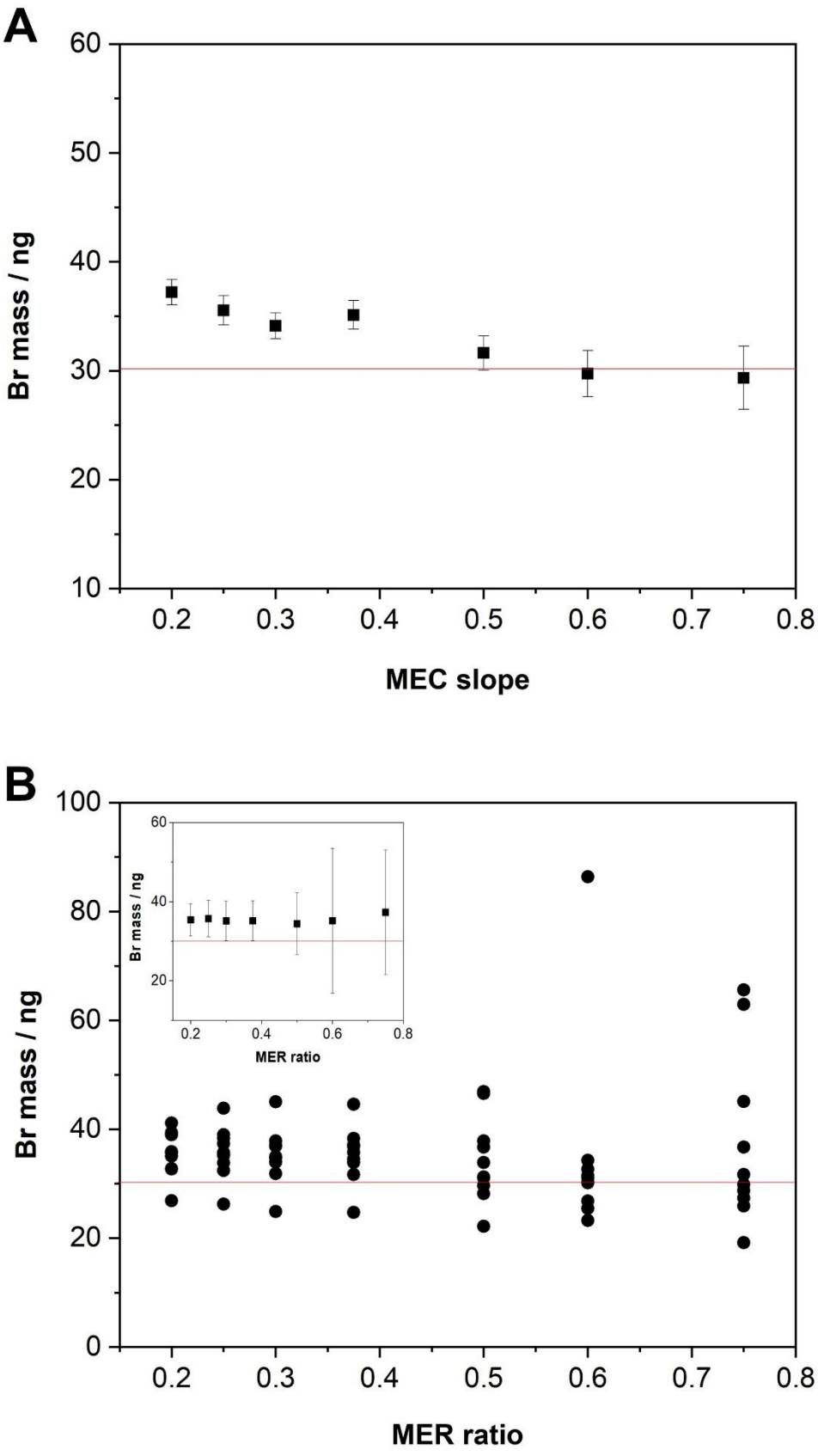
A
Br mass / ng
MEC slope
B
Br mass / ng
MER ratio
Br mass / ng
MER ratio

Figure 6

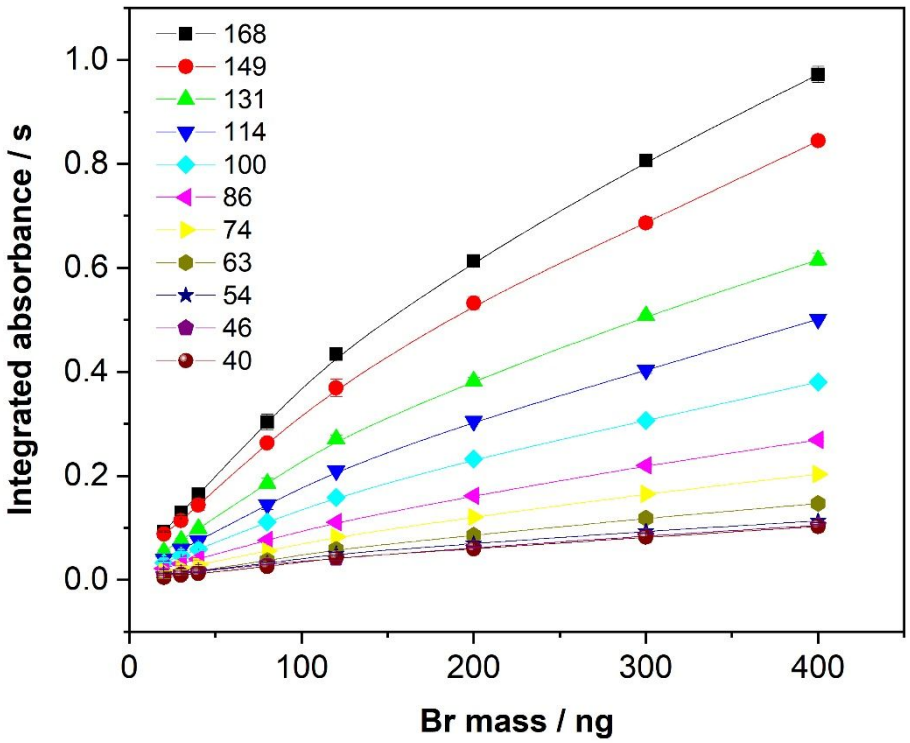
168
149
131
114
100
86
74
63
54
46
40
Integrated absorbance / s
Br mass / ng
0.0
0.2
0.4
0.6
0.8
1.0
0
100
200
300
400

Figure 7

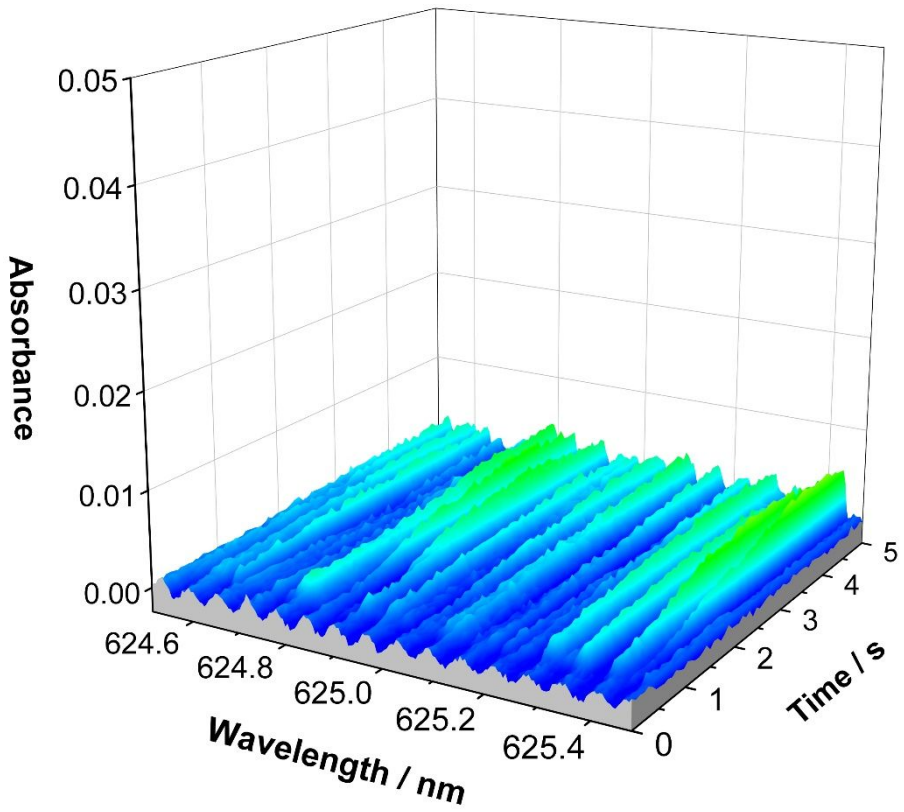
0.05
0.04
0.03
0.02
0.01
0.00
Absorbance
624.6
624.8
625.0
625.2
625.4
Wavelength / nm
0
1
2
3
4
5
Time / s

Figure 8

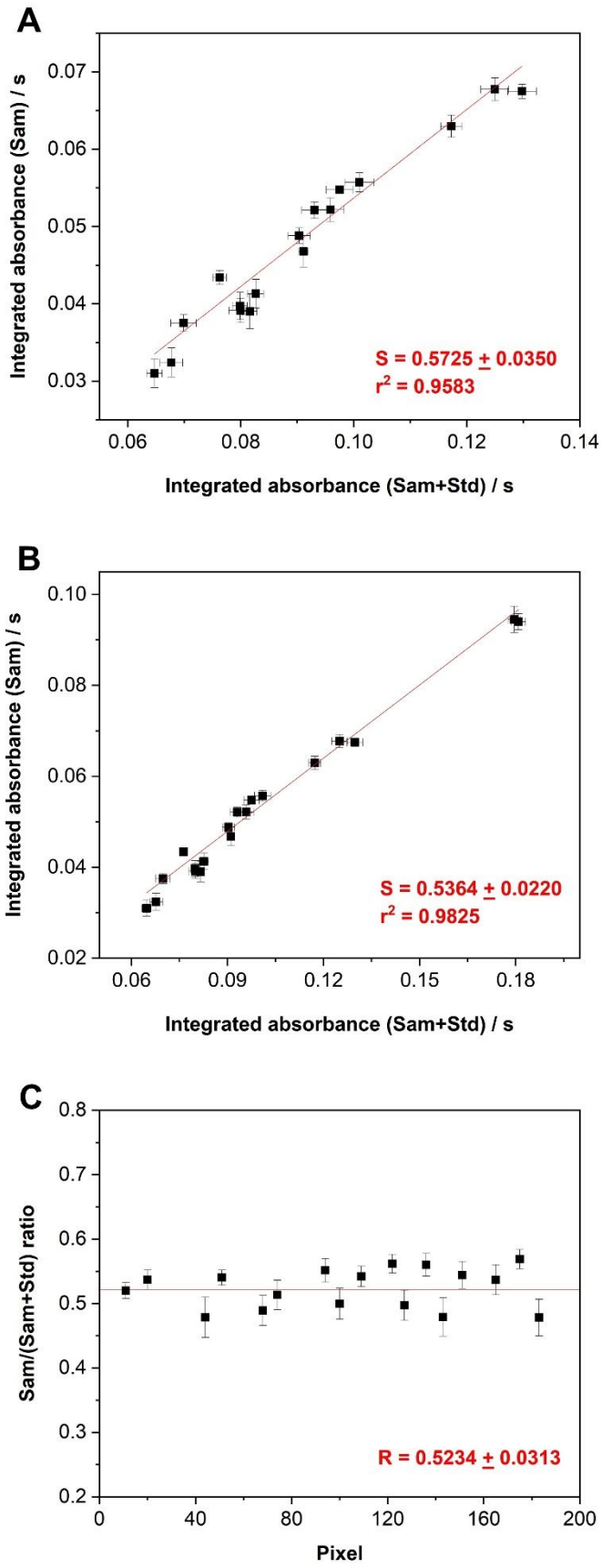
A
Integrated absorbance (Sam) / s
Integrated absorbance (Sam+Std) / s
S = 0.5725 ± 0.0350
r² = 0.9583
B
Integrated absorbance (Sam) / s
Integrated absorbance (Sam+Std) / s
S = 0.5364 ± 0.0220
r² = 0.9825
C
Sam/(Sam+Std) ratio
Pixel
R = 0.5234 ± 0.0313

Figure 9

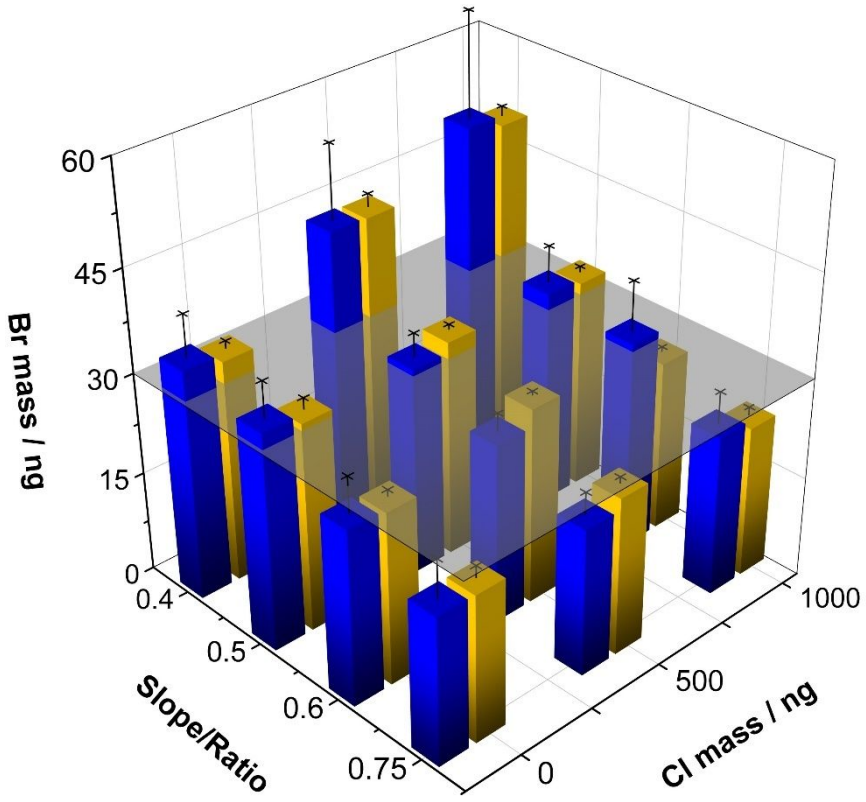
60
45
30
15
0
Br mass / ng
0.4
0.5
0.6
0.75
Slope/Ratio
0
500
1000
Cl mass / ng

Development of equations 8 and 9 from equation 7

$$bias^{\pm}_{CSam}(\%) = \frac{\left\{\frac{(S \pm e_S)}{[1-(S \pm e_S)]}\right\} - \left(\frac{S}{1-S}\right)}{\left(\frac{S}{1-S}\right)} \times 100\% \qquad (7)$$

It can be noticed (see equation 6) that the upper limit of e_S value will lead to the upper limit of e_C and concentration bias, $e_C{}^+$ and $bias^{+}_{CSam}$ respectively. Thus, equation 7 can be further developed as follows.

$$bias^{+}_{CSam}(\%) = \frac{\left\{\frac{(S + e_S)}{[1-(S + e_S)]}\right\} - \left(\frac{S}{1-S}\right)}{\left(\frac{S}{1-S}\right)} \times 100\%$$

$$bias^{+}_{CSam}(\%) = \frac{\left\{\frac{[(S + e_S) \times (1-S)] - [S \times (1-S-e_S)]}{(1-S-e_S) \times (1-S)}\right\}}{\left(\frac{S}{1-S}\right)} \times 100\%$$

$$bias^{+}_{CSam}(\%) = \frac{(S - S^2 + e_S - Se_S - S + S^2 + Se_S)}{(1-S-e_S) \times (1-S)} \times \frac{(1-S)}{S} \times 100\%$$

$$bias^{+}_{CSam}(\%) = \frac{e_S}{S(1-S-e_S)} \times 100\% \qquad (8)$$

The lower limit, $bias^{-}_{CSam}$, can be calculated analogously, resulting in equation 9.

$$bias^{-}_{CSam}(\%) = \frac{\left\{\frac{(S - e_S)}{[1-(S - e_S)]}\right\} - \left(\frac{S}{1-S}\right)}{\left(\frac{S}{1-S}\right)} \times 100\%$$

$$bias^{-}_{CSam}(\%) = \frac{\left\{\frac{[(S - e_S) \times (1-S)] - [S \times (1-S+e_S)]}{(1-S+e_S) \times (1-S)}\right\}}{\left(\frac{S}{1-S}\right)} \times 100\%$$

$$bias^{-}_{CSam}(\%) = \frac{(S - S^2 - e_S + Se_S - S + S^2 - Se_S)}{(1-S+e_S) \times (1-S)} \times \frac{(1-S)}{S} \times 100\%$$

$$bias_{\bar{C}sam}(\%) = \frac{-e_S}{S(1 - S + e_S)} \times 100\% \qquad (9)$$

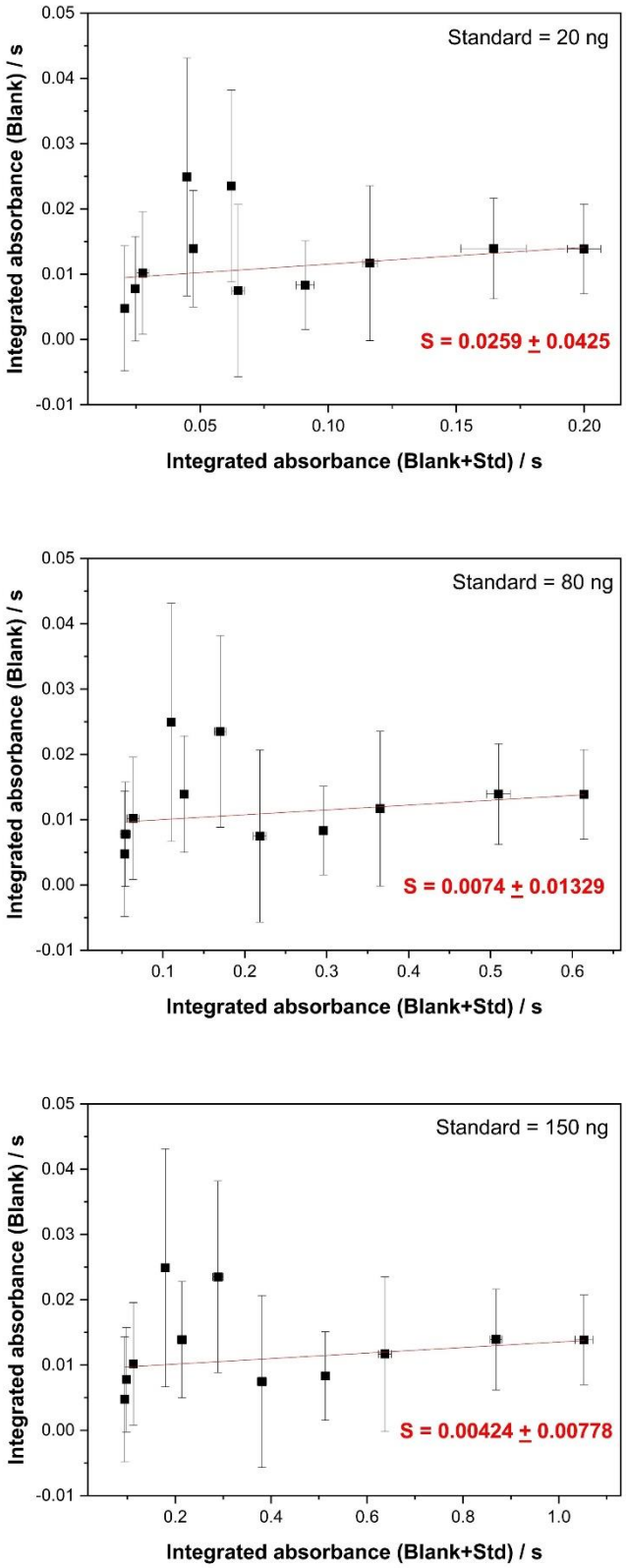

Figure S1. Blank measurements vs. 20, 80 and 150 ng Br spikes using MEC for calculating the LOD and LOQ, as described in equation 13.